

## FREE-SUSPENSION RESIDUAL FLEXIBILITY TESTING OF SPACE STATION PATHFINDER: COMPARISON TO FIXED-BASE RESULTS

Michael L. Tinker \*  
Structural Dynamics and Loads Branch/ED23  
Structures and Dynamics Laboratory  
NASA/Marshall Space Flight Center  
Huntsville, AL 35812

11-10-012

134045

### Abstract

Application of the free-suspension residual flexibility modal test method to the International Space Station Pathfinder structure is described. The Pathfinder, a large structure of the general size and weight of Space Station module elements, was also tested in a large fixed-base fixture to simulate Shuttle Orbiter payload constraints. After correlation of the Pathfinder finite element model to residual flexibility test data, the model was coupled to a fixture model, and constrained modes and frequencies were compared to fixed-base test modes. The residual flexibility model compared very favorably to results of the fixed-base test. This is the first known direct comparison of free-suspension residual flexibility and fixed-base test results for a large structure.

The model correlation approach used by the author for residual flexibility data is presented. Frequency response functions (FRF) for the regions of the structure that interface with the environment (a test fixture or another structure) are shown to be the primary tools for model correlation that distinguish or characterize the residual flexibility approach. A number of critical issues related to use of the structure interface FRF for correlating the model are then identified and discussed, including (1) the requirement of prominent stiffness lines, (2) overcoming problems with measurement noise which makes the antiresonances or minima in the functions difficult to identify, and (3) the use of interface stiffness and lumped mass perturbations to bring the analytical responses into agreement with test data. It is shown that good comparison of analytical-to-experimental FRF is the key to obtaining good agreement of the residual flexibility values.

### Introduction

Fixed-base modal survey tests have traditionally been

\*Aerospace Technologist, Structural Dynamics; Senior Member AIAA

Copyright © 1998 by the American Institute of Aeronautics and Astronautics, Inc. No copyright is asserted in the United States under Title 17, U.S. Code. The U.S. government has a royalty-free license to exercise all rights under the copyright claimed herein for Governmental purposes. All other rights are reserved by the copyright owner.

used in the aerospace industry for refinement of mathematical models of substructures or launch vehicle payloads. This is mainly because the test configuration is designed to match the flight boundary conditions as closely as possible. The measured fixed-interface modes can also be used directly in the well-known Hurty or Craig-Bampton component synthesis methods (Refs. 1-3). However, an adequate fixed-base test fixture is not always available, and the cost of designing and building one may be prohibitive. Test articles are sometimes shipped to a facility where test fixturing exists, but there is considerable inconvenience as well as cost and scheduling problems involved in such a practice. There are also a number of difficulties associated with measurement of modal parameters in fixed-boundary modal tests, in some cases making the approach impractical. For example, as described in Refs. 4 and 5, it is not possible to perform a truly fixed-boundary test due to coupling between the test article and fixture. In addition, the boundary constraints of the test article may not adequately simulate flight conditions, particularly in cases such as Shuttle payloads where some degrees-of-freedom (DOF) at a boundary point are constrained and some DOF are free.

To provide an alternative approach for verifying substructure models, the free-boundary residual flexibility method has been investigated. This approach provides a technique for obtaining fixed-boundary mode shapes for a structure through measurement of (1) free-suspension mode shapes of the overall structure, and (2) frequency response data for the boundary DOF to be constrained in service. Measured free-free data can be utilized in a component mode synthesis approach to derive the constrained data. A residual flexibility value is obtained by measuring or calculating a displacement/force frequency response function (FRF), and subtracting from it the FRF synthesized from mode shapes and frequencies. The value of the remaining function at zero frequency is defined as residual flexibility.

The residual flexibility approach has been treated analytically in considerable detail, as described in Refs. 6-12, but has had limited application to date as a test method (Refs. 13-16). Residual flexibility testing has been used in relatively few cases due to concern over difficulty in performing the required frequency response (FRF) measurements from which residuals are derived. This concern is justified for a number of reasons. Two of these are well-described by Blair (Ref. 16). First, residual flexibilities are very small numbers, typically on the order of  $1.0E-6$  in/lb for translational diagonal terms, and orders of magnitude smaller for off-diagonal values. This presents difficulty in obtaining accurate and noise-free measurements, especially for points removed from the excitation source. A

second difficulty encountered in residual measurements lies in obtaining a clean residual function in the process of subtracting synthesized modal data from a measured response function.

Craig discussed potential problems with the residual flexibility matrix and the associated mass matrix in Ref. 10, pointing out that "...although the residual flexibility method appears to hold the most promise as a CMS (component mode synthesis) method for use with experimentally-acquired data, additional careful study is needed in order to clarify the potential problems and possibilities inherent in the method."

Recent research (Refs. 12, 17-18) has addressed some of the problems associated with residual flexibility measurements and analysis, and helped clarify limits of practical application. It was demonstrated that for accurate residual measurements, drive point FRF (response measured at the excitation point) having prominent stiffness lines in the acceleration/force format are needed. This is because noise in FRF measurement and errors in parameter estimation of modal properties are overcome by the dominant mode(s) of the interface region of the structure, and the associated stiffness line in the FRF. Physically, the dominant stiffness line in an FRF means that the interface region has one or more mode shapes having amplitude much higher than other modes in the frequency band. Or, the drive/response point has a resonant amplitude much higher than the response at other frequencies, somewhat resembling single-degree-of-freedom (SDOF) behavior, and implying a flexible connection to the remaining structure. The lack of such stiffness lines increases measurement errors for residual flexibility values. Interface drive point frequency response functions for many Shuttle Orbiter payloads exhibit dominant stiffness lines, at least for some constraint coordinates, making the residual test approach a good candidate for payload modal tests. Figure 1 shows a Shuttle payload carrier with the trunnion and keel interfaces clearly shown, and in Fig. 2 a drive point response is shown for one of the payload interfaces. The prominent stiffness line is clearly seen in Fig. 2, and the resemblance to SDOF behavior can also be observed.

Difficulties in extracting a residual flexibility value from noisy test data have also been addressed in recent research (Refs. 17-18). It was shown that use of a weighted second order least-squares curve fit of the measured residual function allows identification of residual flexibility that compares very well with predictions for simple structures. That approach also provides an estimate of second order residual mass effects.

### Analytical Background of the Residual Flexibility Method

The technique of using an approximation of the effects of neglected higher order modes, or residual modes, to improve the accuracy of reduced-basis mathematical models was first presented by MacNeal (Ref. 6). In MacNeal's method, a substructure model derived from truncated modal properties was improved by including additional elements derived from first-order static approximations of the effects of higher modes. Rubin (Ref. 7) used a special statics

problem to derive an expression for residual flexibility in a form that is more easily applied in structural dynamic analyses.

### Matrix Formulation

As described in Ref. 7, the flexible-body displacements for a substructure can be written as a first-order approximation of residual effects,

$$\mathbf{u}_f = \mathbf{G}\mathbf{F} = \mathbf{A}^T \mathbf{G}_c \mathbf{A}\mathbf{F} \quad (1)$$

where  $\mathbf{G}$  is the free-free flexibility matrix. The constrained flexibility matrix is  $\mathbf{G}_c$  and the transformation matrix

$\mathbf{A} = \mathbf{I} - \mathbf{M}\Phi_R \mathbf{M}_R^{-1} \Phi_R^T$ . It is noted that  $\mathbf{M}_R$  is the generalized mass associated with the rigid body modes  $\Phi_R$ . If the contribution of modes to be retained is removed from the deflection for the flexible substructure, the residual flexibility matrix  $\mathbf{G}_r$  results, as shown in Eq. (2):

$$\mathbf{u}_{fr} = (\mathbf{G} - \mathbf{G}_n) \mathbf{F} = \mathbf{G}_r \mathbf{F} \quad (2)$$

where  $\mathbf{G}_n = \Phi_n \mathbf{K}_n^{-1} \Phi_n^T$  is the flexibility matrix corresponding to the retained modes.

In Ref. 11, Martinez, et. al, expressed substructure displacements in the form

$$\mathbf{u} = \Phi \mathbf{q} + \mathbf{G}_{rb} \mathbf{F}_b = [\Phi \quad \mathbf{G}_{rb}] \begin{Bmatrix} \mathbf{q} \\ \mathbf{F}_b \end{Bmatrix} \quad (3)$$

where  $\Phi$  is the  $(N \times n)$  matrix of retained or measured modes and  $\mathbf{G}_{rb}$  is a partition of the  $(N \times N)$  residual flexibility matrix defined in Eq. (2). If the displacements are partitioned into interior and boundary or interface degrees of freedom, Eq. (3) becomes

$$\begin{Bmatrix} \mathbf{u}_i \\ \mathbf{u}_b \end{Bmatrix} = \begin{bmatrix} \Phi_i & \mathbf{G}_{rib} \\ \Phi_b & \mathbf{G}_{rbb} \end{bmatrix} \begin{Bmatrix} \mathbf{q} \\ \mathbf{F}_b \end{Bmatrix} \quad (4)$$

By solving the lower partition of Eq. (4) for the boundary forces, and substituting the resulting expression back into Eq. (4), the interior physical displacements are obtained in terms of generalized interior and physical boundary displacements,

$$\mathbf{u}_i = (\Phi_i - \mathbf{G}_{rib} \mathbf{G}_{rbb}^{-1} \Phi_b) \mathbf{q} + \mathbf{G}_{rib} \mathbf{G}_{rbb}^{-1} \mathbf{u}_b \quad (5)$$

Combining Eq. (5) with the identity  $\mathbf{u}_b = \mathbf{u}_b$  yields the desired transformation for substructure displacements,

$$\begin{Bmatrix} \mathbf{u}_i \\ \mathbf{u}_b \end{Bmatrix} = \begin{bmatrix} \Phi_i - \mathbf{G}_{rib} \mathbf{G}_{rbb}^{-1} \Phi_b & \mathbf{G}_{rib} \mathbf{G}_{rbb}^{-1} \\ \mathbf{0} & \mathbf{I} \end{bmatrix} \begin{Bmatrix} \mathbf{q} \\ \mathbf{u}_b \end{Bmatrix} = \mathbf{T} \begin{Bmatrix} \mathbf{q} \\ \mathbf{u}_b \end{Bmatrix} \quad (6)$$

where  $\mathbf{T}$  is an  $(N \times m)$  matrix and  $m = n + n_b$ , the number of retained modes plus the number of boundary dof.

The partitioned form of the undamped equation of motion for a substructure is

$$\begin{bmatrix} \mathbf{M}_{ii} & \mathbf{M}_{ib} \\ \mathbf{M}_{bi} & \mathbf{M}_{bb} \end{bmatrix} \begin{Bmatrix} \ddot{\mathbf{u}}_i \\ \ddot{\mathbf{u}}_b \end{Bmatrix} + \begin{bmatrix} \mathbf{K}_{ii} & \mathbf{K}_{ib} \\ \mathbf{K}_{bi} & \mathbf{K}_{bb} \end{bmatrix} \begin{Bmatrix} \mathbf{u}_i \\ \mathbf{u}_b \end{Bmatrix} = \begin{Bmatrix} \mathbf{0} \\ \mathbf{F}_b \end{Bmatrix} \quad (7)$$

and the corresponding partitioned form of the residual flexibility matrix is

$$\mathbf{G}_r = \begin{bmatrix} \mathbf{G}_{rii} & \mathbf{G}_{rib} \\ \mathbf{G}_{rbi} & \mathbf{G}_{rbb} \end{bmatrix} \quad (8)$$

where  $\mathbf{G}_r$  is to be obtained using frequency response measurements of the free-free test article for the connect coordinates and shaker drive points (Ref. 2), or computed using Eqs. (1) and (2). The retained natural frequencies and mode shapes,  $\omega_n^2$  and  $\Phi_n$ , are to be obtained from a free-boundary modal test, and correspond to subsets of the eigenvalues and eigenvectors of Eq. (7) with  $\mathbf{F} = \mathbf{0}$ . Applying the transformation defined in Eq. (6) to Eq. (7), the substructure reduced equation of motion becomes

$$\bar{\mathbf{M}} \begin{Bmatrix} \ddot{\mathbf{q}} \\ \ddot{\mathbf{u}}_b \end{Bmatrix} + \bar{\mathbf{K}} \begin{Bmatrix} \mathbf{q} \\ \mathbf{u}_b \end{Bmatrix} = \mathbf{T}^T \begin{Bmatrix} \mathbf{0} \\ \mathbf{F}_b \end{Bmatrix} \quad (9)$$

where  $\bar{\mathbf{M}} = \mathbf{T}^T \mathbf{M} \mathbf{T}$  and  $\bar{\mathbf{K}} = \mathbf{T}^T \mathbf{K} \mathbf{T}$ . Martinez, et. al (Ref. 11) showed that

$$\bar{\mathbf{M}} = \begin{bmatrix} \mathbf{I}_{nn} + \Phi_{nb}^T \mathbf{J}_{bb} \Phi_{nb} & -\Phi_{nb}^T \mathbf{J}_{bb} \\ \text{sym.} & \mathbf{J}_{bb} \end{bmatrix}$$

$$\bar{\mathbf{K}} = \begin{bmatrix} \Omega_{nn}^2 + \Phi_{nb}^T \mathbf{G}_{rbb}^{-1} \Phi_{nb} & -\Phi_{nb}^T \mathbf{G}_{rbb}^{-1} \\ \text{sym.} & \mathbf{G}_{rbb}^{-1} \end{bmatrix} \quad (10)$$

where  $\Omega_{nn}$  is the diagonal matrix of retained or measured frequencies  $\omega_n$ , and  $\Phi_{nb}$  is the boundary partition of the retained modes. Also in Eq. (10),  $\mathbf{J}_{bb} = \mathbf{G}_{rbb}^{-1}$

$\mathbf{H}_{bb} \mathbf{G}_{rbb}^{-1}$  and  $\mathbf{H}_{bb} = \mathbf{G}_{rb}^T \mathbf{M} \mathbf{G}_{rb}$ , where  $\mathbf{G}_{rb} = [\mathbf{G}_{rib} \quad \mathbf{G}_{rbb}]^T$ . Residual mass effects are contained in the boundary partition  $\mathbf{H}_{bb}$ , and the full residual mass matrix is given by

$$\mathbf{H}_r = \mathbf{G}_r^T \mathbf{M} \mathbf{G}_r \quad (11)$$

In order to verify an ideally-constrained model, the corresponding constrained modes must be derived. As discussed in Admire, et al. (Ref. 12), this is accomplished using the present formulation by striking the rows and columns of the matrices in Eq. (10) for boundary dof, yielding

$$\bar{\mathbf{M}}_{nn} \ddot{\mathbf{q}} + \bar{\mathbf{K}}_{nn} \mathbf{q} = \mathbf{0} \quad (12)$$

where  $\bar{\mathbf{M}}_{nn} = [\mathbf{I}_{nn} + \Phi_{nb}^T \mathbf{J}_{bb} \Phi_{nb}]$  and  $\bar{\mathbf{K}}_{nn} = [\Omega_{nn}^2 + \Phi_{nb}^T \mathbf{G}_{rbb}^{-1} \Phi_{nb}]$ , and both matrices are  $(n \times n)$ . The eigenvalues  $\omega_c^2$  calculated from Eq. (12) are the constrained frequencies, and the constrained modes are obtained by assembling the eigenvectors from Eq. (12),  $\Phi_{nn}$ , into an  $(m \times n)$  matrix and premultiplying by  $\mathbf{T}$  from Eq. (6):

$$\Phi_c = \mathbf{T} \begin{bmatrix} \Phi_{nn} \\ \mathbf{0} \end{bmatrix} \quad (13)$$

Since  $\mathbf{T}$  is  $(N \times m)$  and the partitioned mode shape matrix is  $(m \times n)$ , an  $(N \times n)$  matrix of constrained modes is obtained. The frequencies and mode shapes for the constrained structure,  $\omega_c$  and  $\Phi_c$ , are used to obtain a verified constrained mathematical model.

To derive modes of a structure constrained in a test fixture, the mass and stiffness matrices described in Eq. (10) must be coupled to the fixture model. Resulting frequencies can be compared directly to the fixed-base test, but the mode shapes require back-transformation and partitioning before comparison to test.

### Frequency Response Function Formulation

To provide an efficient means of comparing test residual measurements with analysis, the frequency response function (FRF) approach as presented by Rubin (Ref. 7) was utilized. In this method which is applicable to both analytical and test data, the displacement is written as a function of frequency,

$$\mathbf{U}(\omega) = \mathbf{Y}(\omega) \mathbf{F}(\omega) \quad (14)$$

where  $\mathbf{Y}$  is the FRF matrix and  $\mathbf{F}$  is the applied force as function of frequency. The residual FRF matrix, or residual function matrix as it will be denoted in this paper, is

obtained by subtracting from the full FRF in Eq. (14) the modal FRF containing the rigid body modes and elastic free-free modes that are to be retained. The undamped modal FRF matrix is given by

$$\mathbf{Y}_m(\omega) = -\Phi_R \frac{1}{\omega^2} \mathbf{M}_R^{-1} \Phi_R^T + \Phi_n \Lambda_n^{-1} \mathbf{M}_n^{-1} \Phi_n^T \quad (15)$$

where  $\mathbf{M}_n$  is the generalized mass associated with the retained modes  $\Phi_n$ , and  $\Lambda_n$  is the diagonal matrix  $\omega_n^2 - \omega^2$ . The residual function matrix becomes

$$\mathbf{Y}_r(\omega) = \mathbf{Y}(\omega) - \mathbf{Y}_m(\omega) \quad (16)$$

which can be approximated over the frequency range of interest by the undamped form

$$\mathbf{Y}_r(\omega) = \mathbf{G}_r + \omega^2 \mathbf{H}_r \quad (17)$$

corresponding to Eqs. (2) and (11). For comparison of residual flexibility values, the undamped forms of Eqs. (15)-(17) should be sufficient. However, if analytical and test FRFs are being compared, damping should be included. In that case,  $\Lambda_n = \omega_n^2 + i 2\zeta_n \omega \omega_n - \omega^2$  in Eq. (15) and the residual function matrix takes the form

$$\mathbf{Y}_r(\omega) = \mathbf{G}_r + \omega^2 \mathbf{H}_r - i \omega \mathbf{B}_r \quad (18)$$

For practical computations, residual functions are obtained individually rather than in matrix form. It is important to note that the FRF and residual functions described here are in displacement/force format. Residual flexibility for a particular residual function is the value of the function at zero frequency, as can be seen from Eqs. (17) and (18). Each  $\mathbf{G}_r$  determined in this way is equal to the corresponding value from Eq. (8). Bookout (Ref. 18) describes a technique for curve-fitting of noisy experimental residual functions to estimate residual flexibility values. In the following sections, application of the residual flexibility approach is described for the Space Station Pathfinder structure, which has prominent interfaces for constraining or coupling to the environment. As stated in the Introduction, this is a requirement for obtaining accurate experimental residual flexibility values.

### Application Of Method to the International Space Station Pathfinder

Free-boundary testing and model correlation activities for the Pathfinder structure (Fig. 3) provided tremendous insight into residual flexibility measurement procedures and achievable accuracy. The desired end result was to compare constrained mode shapes derived using free-free residual

flexibility testing to fixed-base test results. To the knowledge of the author, this has not been done previously for a large structure.

### Characteristics of Free-Boundary Test Data

It should first be pointed out that the testing described here had to be done in a less-than-optimum situation and environment, in that the suspension of the test article and the measurements were done quickly. In other words, the testing had to be done "on the fly", without the benefit of comprehensive pre-test analysis. A short amount of time was available during a period of fixed-base testing of the Pathfinder for doing free-free measurements.

The Pathfinder was suspended using a large crane. A series of bungee cords was used to make the supports as soft as possible, but still able to safely support the 28,000 lb test article. Free-free mode shape measurements were obtained using shaker excitation. It was discovered that the suspension system was more stiff than desirable, and that it contaminated the first elastic mode to some extent. However, this problem was worked around quite easily by including the elastic suspension cords in the model.

Trunnion and keel interface response data, which was initially obtained using impact hammer excitation, presented considerable difficulty, and was found to be very noisy in the antiresonance regions (Fig. 5). Softer hammer tips were utilized in efforts to improve the data, but this had little effect other than to degrade the resolution of the resonances or peaks. In further attempts to obtain cleaner measurements, shaker excitation was examined, but was found to provide little or no improvement in the antiresonances. The shaker did provide better resolution of the peaks, however. Finally, the data was accepted as the best that could be obtained in the amount of time available, and model correlation was initiated as described in the following sections.

### Correlation of Free-Free Mode Shapes and Frequencies

The first step in the process was to update the Pathfinder finite element model to obtain the best agreement possible with test free-free modes. Mode shape correlation procedures for residual flexibility testing are essentially the same as other free-boundary modal testing. A goal of 2 percent frequency error was established when it became clear that such a goal was realistic. Since it was not known how accurate the residual flexibility model had to be to yield constrained frequencies within 5 percent of test, additional accuracy was desirable. It has not yet been determined if the standard 5 percent error limit on frequency is sufficient for free-suspension modes when using them to derive constrained modes.

Visual inspection of animated analytical modes quickly showed that the trunnion support structures on the upper beams of the Pathfinder were rocking about the x-axis at much lower frequency than in the test. Increasing the torsion constant of the upper beams successfully moved the trunnion rocking modes to higher frequencies. However, it was not possible to complete correlation of the upper beam torsional properties until frequency response functions (FRF) were examined. That work is described later in this section.

Figure 4 shows several experimental free-boundary mode shapes. Due to the relatively simple geometry of the test article, it was possible to quickly identify model changes for pure bending modes in the lateral (y) and vertical (z) directions. For example, the y- and z-bending modes were correlated by increasing or decreasing (by up to 10 percent as a limit) the area moments of inertia for the upper and lower long beams in each bending direction. The second y-bending mode and an x-y shearing mode were also driven by the long beam y-bending area moment of inertia. Other modes were also visually inspected to identify critical parts of the structure and properties (I or J) to modify. As further examples, the two torsion modes (shapes 1 and 6 in Fig. 4) were controlled at least partially by the torsion constant of the center upper beam. Due to the fact that correlating one mode often resulted in worse agreement with test for other modes, considerable iteration was required for the final correlation of all 9 elastic modes. As shown in Table 1, the 2 percent frequency error goal was achieved for the 9 elastic mode shapes. Good orthogonality checks were also achieved, with the worst value being near 0.93.

Difficulty was encountered in correlating the tenth elastic mode to the test data. The mode was characterized by x-direction motion of the lower central portion of the Pathfinder. An explanation for the relatively poor frequency correlation (near 7 percent error) is that the upper beams were about 21 in. deep in the z-direction. Diagonal beams welded to the bottom surfaces of the upper beams, as can be seen in Fig. 3, may have local flexibility that can only be characterized using detailed plate models for the upper beams.

#### **Updating for Boundary Frequency Response**

The next step was to examine the drive point response functions for the trunnions (upper beam interfaces) and keel (interface on lower beam). It is again noted that "drive point" refers to excitation and response occurring at the same point on the structure. Hammer impacts were used to excite the structure. In Fig. 5 the analytical FRF before updating is compared to test for the keel. Noisy data is apparent for the measured response near the antiresonance as discussed earlier. Upon initial inspection of this data, it was concluded that model correlation would be extremely difficult for the antiresonances. The impact of noise in the data on model correlation will be addressed in the next paragraph.

In the updating process, it was quickly found that the torsion constant of the upper beams in the vicinity of the trunnions was the sensitive parameter for correlating the z-direction FRF. Increasing the torsion constants (J) for the upper beams brought the trunnion z-direction response antiresonances into good agreement with test, and the addition of lumped mass at the trunnion supports (for bolts and welds) improved the peak or resonant frequency correlation. Similarly, increasing J for the lower beam (near the keel) brought the keel y-response antiresonance into good agreement with test. Figure 6 shows the test and analysis FRF after model updating for the keel y-direction. Early in the FRF updating process, as stated in the previous paragraph, it was thought that the noisy test data near antiresonances would present severe problems, but this was not the case. Visual comparison of overlaid test/analysis FRF was sufficient for determining when good antiresonance

agreement had been achieved. Inspection of the response functions at frequencies slightly above and below the antiresonance revealed when a good correlation had been obtained.

The trunnion x-direction responses presented particular difficulty for model correlation due to the lack of any visible stiffness lines. This made it difficult to target modeling changes. In fact, all that was done to update these FRF was to refine the mode frequencies as much as possible, as discussed at the beginning of this section. Poor agreement was observed above 60 Hz, corresponding to the inability to correlate the tenth mode (62.84 Hz in test) with good accuracy.

The approach taken in this paper for test/analysis correlation of residual flexibility values was to update the model to obtain good agreement between analytical and measured drive point response functions for the interfaces, and then to compare the residual values. It has been found that such an approach yields good agreement of the model with measured residual flexibilities. However, the accuracy requirement appears to be quite stringent. The experience of the author is that the analytical FRF must lie virtually on top of the measured data (in visual comparisons) for the analytical residual flexibility values to be within a few percent of the test values. Agreement of this quality may not be possible in many applications. It can be seen from Figs. 5-6 that excellent visual comparisons were obtained for the FRF, and in Table 2 the test and analysis residual flexibility values are compared for all the interfaces of the Pathfinder. The poor agreement for the x-direction residuals is due to the lack of stiffness lines in the FRF, as explained previously, and the resulting inaccurate curve fits to obtain experimental values.

#### **Comparison of Derived Constrained Modes with Fixed-Base Test Data**

Following correlation of free-free modes and frequencies, interface drive-point FRF, and residual flexibility values, the free-boundary finite element model was coupled to a model of the Universal Test Fixture (UTF, Fig. 7). This test fixture was used in the constrained test of the Pathfinder. As described by Tinker (Ref. 19), the UTF utilizes flexure mechanisms to simulate Shuttle Orbiter payload constraints. The flexures are very stiff in the constrained directions and soft in other coordinates. However, a 6-DOF connection is made at each flexure, and undesirable constraints exist in DOF that are free in the Shuttle Orbiter. The flexure system still represents the state-of-the-art for constrained modal testing of Shuttle payloads.

It is noted here that the Pathfinder model was not correlated in rotational DOF for any of the interface FRF, nor was the keel correlated for x- or z-responses, and two trunnions were not correlated in the x-direction. That is, only the Shuttle Orbiter-constrained DOF were examined in detail in the correlation activity. In future applications of free-free testing, it may become necessary to correlate the "unconstrained" translational directions if results are to be compared to fixed-base testing. Rotational measurements are still generally impractical and will not likely be considered.

Table 3 shows the analytical constrained frequency and mode comparisons to test data. Table 4 describes similar comparisons for a model that was independently correlated by Boeing Defense and Space Group (Phillips, Ref. 20) to the fixed-base test directly. These tables illustrate clearly that the free-free correlation to mode shapes, interface FRF, and residual flexibility values yielded a model that compares very favorably with a model correlated in traditional fashion to fixed-base data. In both cases, the frequency error is high for modes 7 and 10. The large frequency error in mode 7 may well be related to the difficulty in correlating the tenth free-free mode discussed earlier in this section. It was stated in relation to the tenth free-boundary mode that a detailed plate model could be required to properly account for flexibility at the diagonal beam connections to the upper beams (Fig. 3).

The last step in the process was to develop a residual flexibility model from the updated finite element model and to repeat the comparison with fixed-base modal data. This reduced model consisted of 15 free-free modes (including rigid-body modes) and 30 residual flexibility values representing the 30 interface DOF with the test fixture. Equation (10) shows the form of the mass and stiffness matrices for the residual flexibility model. After coupling to a Craig-Bampton reduced model (Ref. 3) of the test fixture, the constrained frequencies and mode shapes were obtained. It is noted that back-transformation of the modes was required before orthogonality comparisons could be made with test. Table 5 again demonstrates good agreement with constrained test modes and frequencies. The residual flexibility model shows little loss in accuracy in comparison to the finite element model. Frequency error for the second mode is higher, while for other modes the error is lower than for the finite element model.

### Summary and Conclusions

This paper has described the application of the residual flexibility test/analysis method to a large, very heavy structure of the general size and weight of Space Station modules. Measurement quality was addressed, and the method was found to be reasonably robust with regard to noise in the interface response measurements. The finite element model updating procedure for the method as practiced by the author was discussed in detail. First, the model was correlated to free-free mode shapes in the traditional manner. Next, the interface drive-point frequency response functions were correlated to the measured functions. Finally, the residual flexibility values were compared.

The accuracy requirement for the FRF comparison is stringent for obtaining accurate residual values. If the accuracy of analytical residual flexibility values is unacceptable, i.e., not within errors of about 10-15 percent, the model can be further modified in the interface regions to provide better agreement between the test/analysis response functions.

In conclusion, it has been shown that the free-boundary test/updates process yielded a model that compared very favorably with constrained test data, and with a model correlated directly to fixed-base test data. This direct comparison of residual flexibility results with fixed-base

testing is very significant. The work described in this paper has addressed further the measurement and model updating requirements for application of the residual flexibility technique. The method is clearly applicable for cases where the test article has interface drive-point frequency response functions with prominent stiffness lines. In such cases, experimental residual values are easily extracted, and modeling changes are often identifiable in a straightforward manner. The absence of stiffness lines in the response functions complicates model updating, because it is not readily apparent what part of the structure should be modified. Model improvements in such cases may be limited to further refinement of the free-free modes and frequencies to obtain smaller frequency errors.

### Acknowledgments

Tim Driskill, Kathy Chandler, and Blaine Anderson of the Dynamics Test Branch at Marshall Space Flight Center are acknowledged for their work in providing modal and frequency response test data used in this study.

### References

1. Hurty, W. C., "Dynamic Analysis of Structural Systems Using Component Modes," *AIAA Journal*, Vol. 3, Apr. 1965, pp. 678-685.
2. Hurty, W. C., Collins, J. D., and Hart, G. C., "Dynamic Analysis of Large Structures by Modal Synthesis Techniques," *Computers and Structures*, Vol. 1, Dec. 1971, pp. 535-563.
3. Craig, R. R., and Bampton, M. C., "Coupling of Substructures for Dynamic Analyses," *AIAA Journal*, Vol. 6, July 1968, pp. 1313-1319.
4. Coleman, A. D., Driskill, T. C., Anderson, J. B., and Brown, D. L., "A Mass Additive Technique for Modal Testing as Applied to the Space Shuttle ASTRO-1 Payload," *Proceedings of the 6th International Modal Analysis Conference*, February 1988, pp. 154-159.
5. Admire, J. R., Tinker, M. L., and Ivey, E. W., "Mass-Additive Modal Test Method for Verification of Constrained Structural Models," *Proceedings of the 10th International Modal Analysis Conference*, February 1992.
6. MacNeal, R. H., "A Hybrid Method of Component Mode Synthesis", *Computers and Structures*, Vol. 1, 1971, pp. 581-601.
7. Rubin, S., "Improved Component Mode Representation for Structural Dynamic Analysis", *AIAA Journal*, Vol. 13, 1975, pp. 995-1006.
8. Craig, R. R., Jr., and Chang, C.-J., "On the Use of Attachment Modes in Substructure Coupling for Dynamic Analysis", *Proceedings of the 18th Structures, Structural Dynamics and Materials Conference*, March 1977, pp. 89-99.
9. Craig, R. R., Jr., *Structural Dynamics--An Introduction to Computer Methods*, John Wiley and Sons, New York, 1981, pp. 482-492.
10. Craig, R. R., Jr., "A Review of Time-Domain and Frequency-Domain Component Mode Synthesis

Methods", Combined Experimental/Analytical Modeling of Dynamic Structural Systems, AMD-Vol. 67, American Society of Mechanical Engineers, New York, 1985, pp. 1-30.

11. Martinez, D. R., Carne, T. G. and Miller, A. K., "Combined Experimental/Analytical Modeling Using Component Mode Synthesis", Proceedings of the 25th Structures, Structural Dynamics and Materials Conference, May 1984, pp. 140-152.

12. Admire, J. R., Ivey, E. W., and Tinker, M. L., "Residual Flexibility Test Method for Verification of Constrained Structural Models", AIAA Journal, Vol. 32, No. 1, Jan. 1994, pp. 170-175. Also Proceedings of the 33rd Structures, Structural Dynamics, and Materials Conference, April 1992, pp. 1614-1622.

13. Flanigan, C. C., "Test-Analysis Correlation of the Transfer Orbit Stage Modal Survey", Report 40864-8, Oct. 1988, SDRC, Inc., San Diego, CA.

14. Klosterman, A. L., and Lemon, J. R., "Dynamic Design Analysis via the Building Block Approach", Shock and Vibration Bulletin, No. 42, Pt. 1, Jan. 1972, pp. 97-104.

15. Smith, K., and Peng, C. Y., "SIR-C Antenna Mechanical System Modal Test and Model Correlation Report", JPL D-10694, Vol. 1, Jet Propulsion Laboratory, Pasadena, CA, April, 1993.

16. Blair, M. A., "Interface Characterization Modal Test Techniques," EM ATTIC 003, NASA Contract NAS8-38251 Final Report, Lockheed Missiles and Space Company, Sunnyvale, CA, Nov. 1991.

17. Tinker, M. L., and Bookout, P. S., "Measurement of Residual Flexibility for Substructures Having Prominent Flexible Interfaces," AIAA-94-1566-CP, Proceedings of the 35th Structures, Structural Dynamics, and Materials Conference, April 1994, pp. 1944-1958.

18. Bookout, P. S., "Statistically Generated Weighted Curve Fit of Residual Functions", Proceedings of the 64th Shock and Vibration Symposium, Oct. 1993, Shock and Vibration Information Analysis Center, Arlington, VA, pp. 422-431.

19. Tinker, M. L., 1995, "Modal Vibration Test Facilities and Methods for Space Station Modules," AIAA Paper 95-1295.

20. Phillips, E. B., "T1297 Pathfinder Flexure Based Modal Test Correlation Results," Report 2-8H23-SGD-120/96, Boeing Defense and Space Group, Huntsville, AL, Dec. 1996.

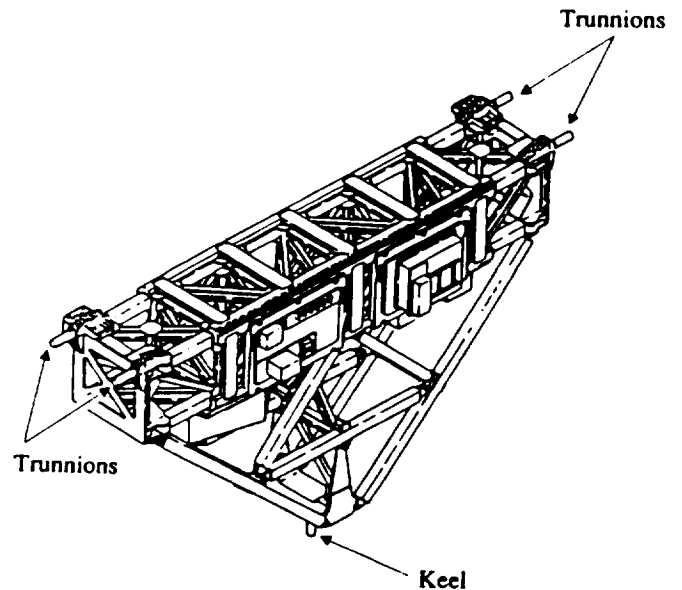


Figure 1. Shuttle Payload Carrier

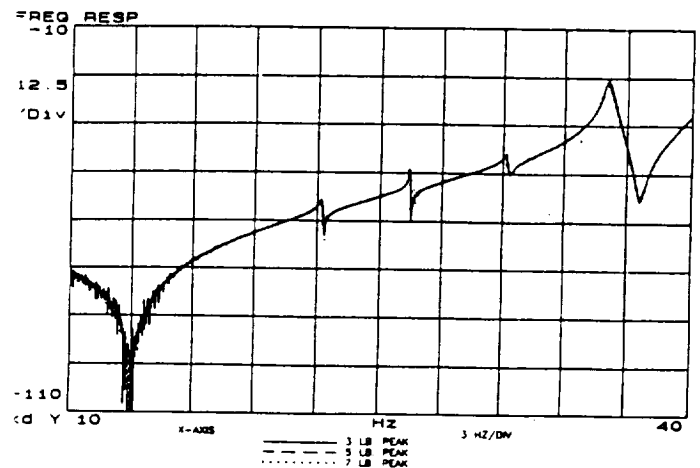


Figure 2. Interface Drive-Point Frequency Response for Shuttle Payload

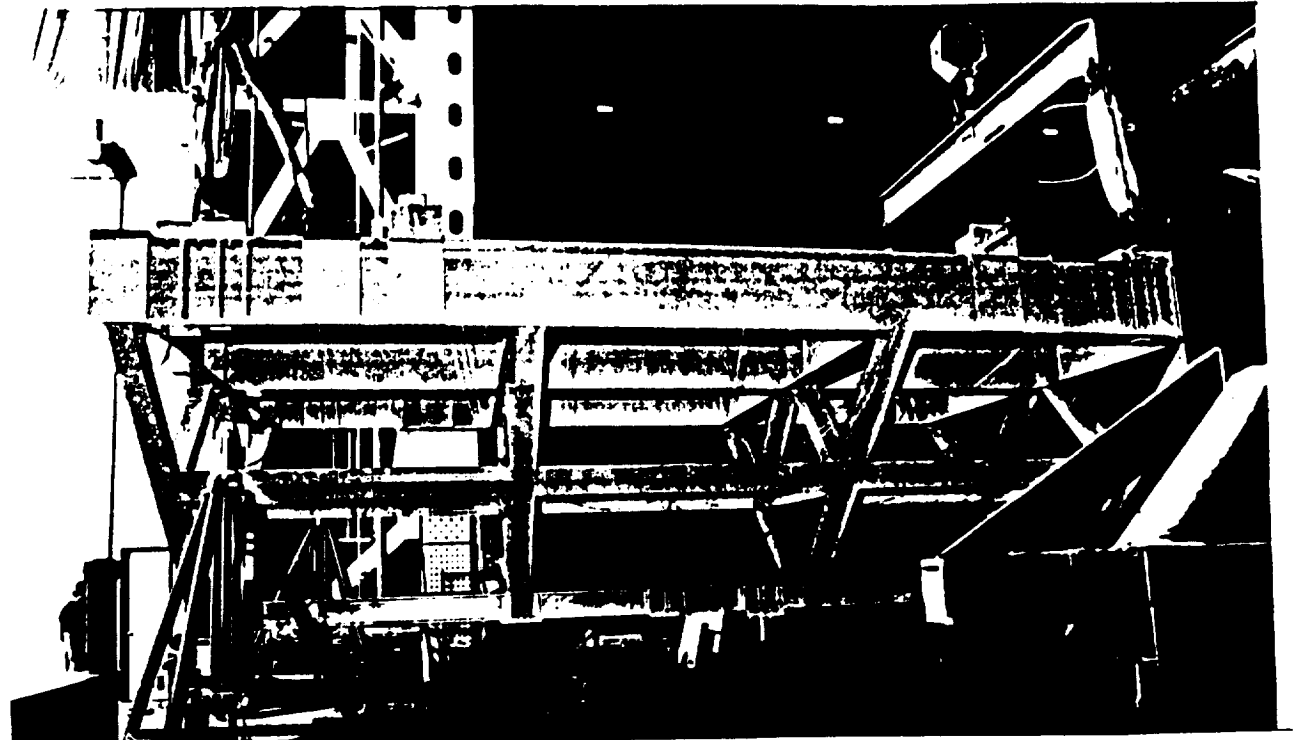


Figure 3. Space Station Pathfinder In Modal Test Configuration

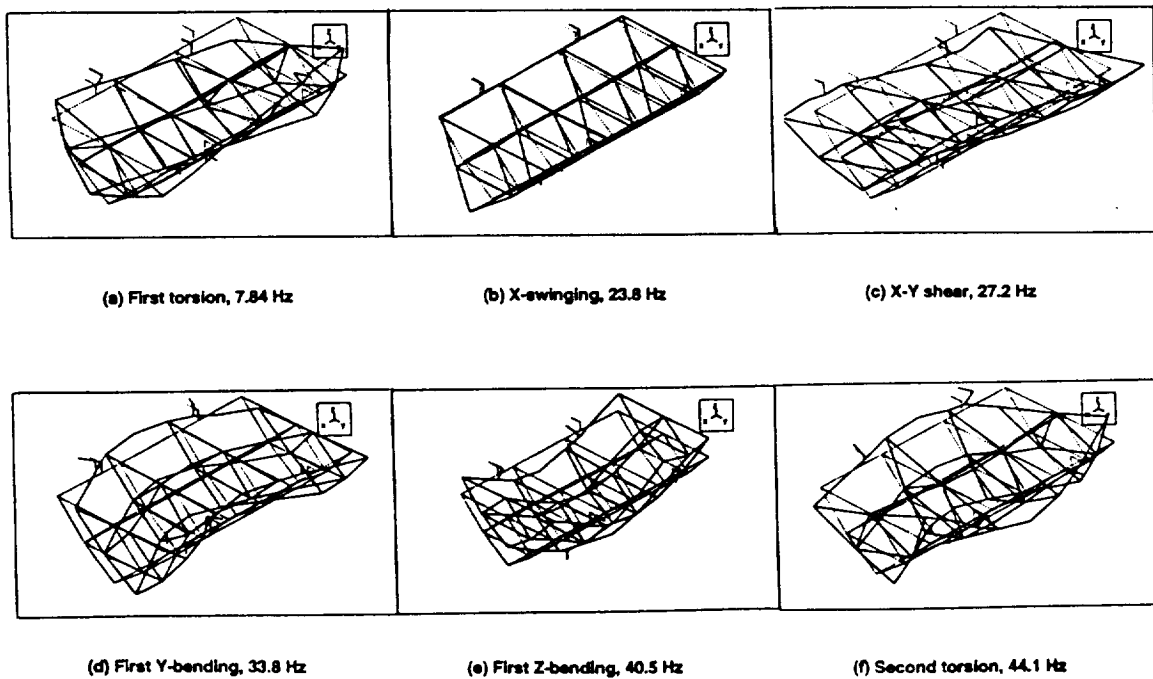


Figure 4. Experimental Free-Free Mode Shapes for Pathfinder

**Table 1. Post-Correlation Comparison of Test and Analytical Free-Free Modes for Space Station Pathfinder**

Mode No.	Test Freq.	Anal. Freq.	Percent Error	Mode Orthog.
1	7.84	7.68	-1.99	.98674
2	23.84	23.50	-1.46	-.99687
3	27.15	26.70	-1.65	.99443
4	33.78	34.33	1.61	-.99366
5	40.45	40.00	-1.12	.99628
6	44.10	44.60	1.15	.99062
7	53.41	53.98	1.06	.99481
8	59.22	59.20	-0.04	.92821
9	60.60	60.82	0.36	.99415

**Table 2. Residual Flexibility Values for Pathfinder, After Model Updates for Trunnions and Keel (9 elastic free modes)**

Model Loc.	Test Residuals, in/lb	Anal. Res. After Updates, in/lb	Percent Error
43Y	8.8047E-06	8.4959E-06	-3.51
44Z	2.9883E-06	2.9958E-06	0.25
45X	1.0674E-06**	1.0677E-06	---
45Z	2.5723E-06	2.8873E-06	12.25
46Z	2.7196E-06	2.6947E-06	-0.92
47X	4.1840E-07**	1.2492E-06	---
47Z	2.7966E-06	3.1298E-06	11.91

\*\*Confidence in experimental residual flexibility values for the X-direction is low, because of noisy data and lack of prominent stiffness lines.

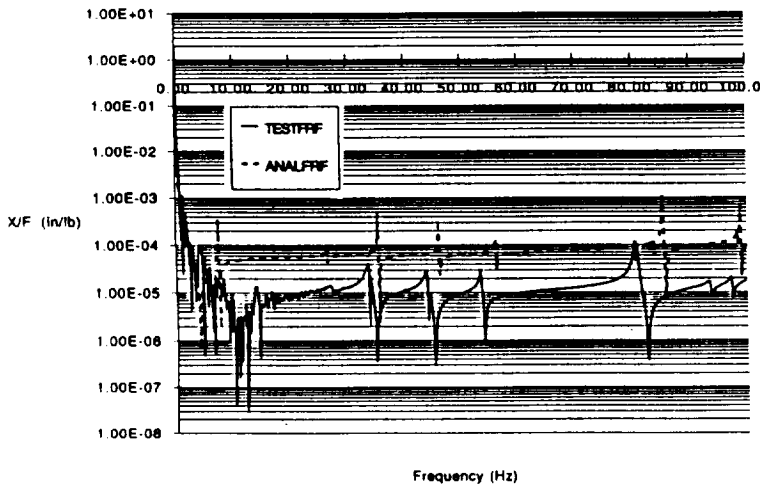


**Figure 5. Test/Analysis Keel Interface Y-Responses Compared Before Model Correlation**

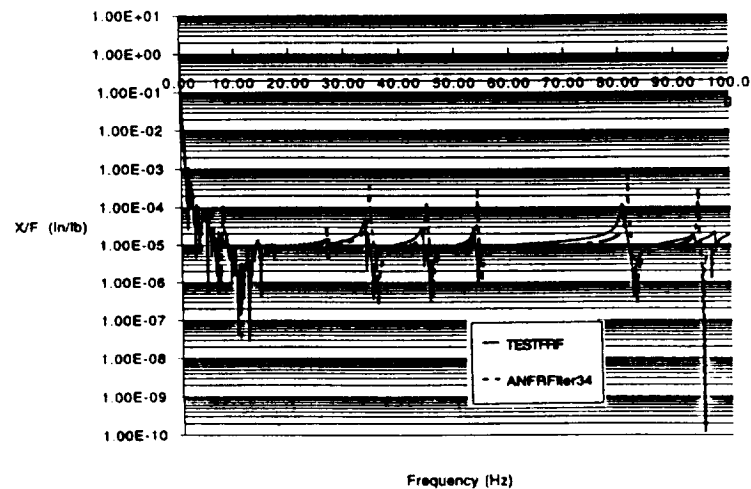
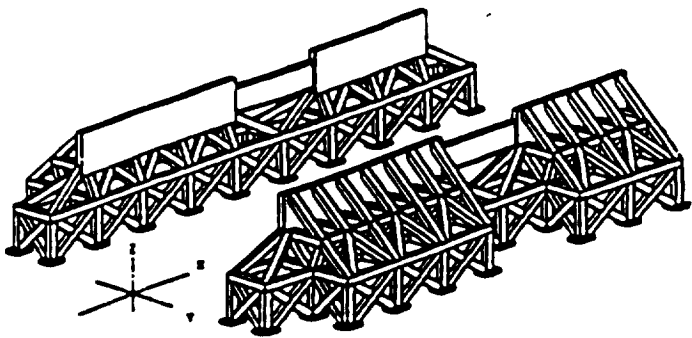
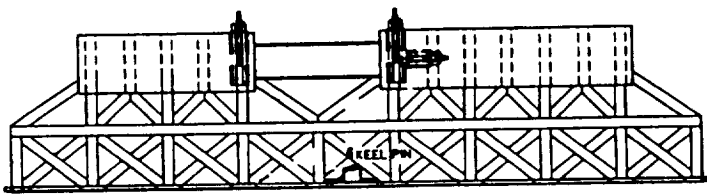


**Figure 6. Keel Test/Analysis Interface Y-Responses Compared After Model Updates**



(a) Strongback Structures



(b) Fixture with Flexure Interface Mechanisms

Figure 7. Universal Test Fixture for Shuttle Payloads

Table 4. Comparison of Test/Analysis Constrained-Boundary Modes for Fixed-Base Test Configuration; Model Tuned Directly to Constrained Test Data

Test Mode No.	Test Freq.	Anal. Mode No.	Anal. Freq.	Percent Error	Mode Orthog.
1	7.46	1	7.22	-3.26	1.00
2	13.28	2	13.88	4.47	-0.99
3	14.83	3	14.81	-0.11	-0.98
4	21.15	4	21.74	2.78	-0.95
5	22.96	5	22.53	-1.83	0.98
6	26.84	6	26.71	-0.48	0.99
7	27.55	7	30.90	12.14	-0.95
8	31.04	8	32.18	3.67	0.99
9	34.25	9	35.01	2.22	0.96
10	39.71	11	45.24	13.94	-0.92
11	42.70	10	43.67	2.27	0.98

Table 3. Comparison of Constrained-Boundary Modes from Constrained Test and Derived from Model Correlated to Free-Free Test for Space Station Pathfinder

Test Mode No.	Test Freq.	Anal. Mode No.	Derived Anal. Freq.	Percent Error	Mode Orthog.
1	7.46	1	7.64	2.28	.99789
2	13.28	2	14.29	7.52	-.99149
3	14.83	3	15.31	3.24	.98658
4	21.15	4	22.23	5.11	-.96187
5	22.96	5	23.54	2.53	.98309
6	26.84	6	28.01	4.36	.98533
7	27.55	7	30.17	9.51	-.95029
8	31.04	8	32.18	3.67	-.98883
9	34.25	9	35.71	4.26	.97942
10	39.71	11	43.59	9.77	-.95655
11	42.70	10	42.58	-0.28	-.98460

Table 5. Comparison of Pathfinder Constrained-Boundary Modes from Constrained Test and Derived from Residual Flexibility Model

Test Mode No.	Test Freq.	Anal. Mode No.	Derived Anal. Freq.	Percent Error	Mode Orthog.
1	7.46	1	7.51	0.67	.99667
2	13.28	2	14.43	8.66	-.99076
3	14.83	3	15.22	2.63	-.98408
4	21.15	4	22.15	4.73	-.96753
5	22.96	5	22.99	0.13	.98327
6	26.84	6	28.10	4.69	.96414
7	27.55	7	30.12	9.33	.94862
8	31.04	8	31.37	1.06	-.97947
9	34.25	9	35.29	3.04	.98262
10	39.71	11	43.15	8.66	-.95861
11	42.70	10	42.63	-0.16	-.97709